High-Fidelity Numerical Wave Tank Verification & Validation Study: Wave Generation Through Paddle Motion

Preprint

T.T. Tran,[1] B.J. Meuris,[2] C. Chartrand,[2] J. Davidson,[3] J. Andersen,[4] C. Eskilsson,[4] M.B. Kramer,[4,5] G. Papadakis,[6] and K. Nielsen[7]

1 National Renewable Energy Laboratory
2 Sandia National Laboratories
3 Basque Center for Applied Mathematics
4 Aalborg University
5 Floating Power Plant
6 National Technical University of Athens
7 Ramboll Group A/S

Presented at 6th International Conference on Renewable Energies Offshore
Lisbon, Portugal
November 19–21, 2024

NREL is a national laboratory of the U.S. Department of Energy
Office of Energy Efficiency & Renewable Energy
Operated by the Alliance for Sustainable Energy, LLC

This report is available at no cost from the National Renewable Energy Laboratory (NREL) at www.nrel.gov/publications.

Contract No. DE-AC36-08GO28308

Conference Paper
NREL/CP-5700-90950
December 2024

High-Fidelity Numerical Wave Tank Verification & Validation Study: Wave Generation Through Paddle Motion

Preprint

T.T. Tran,[1] B.J. Meuris,[2] C. Chartrand,[2] J. Davidson,[3] J. Andersen,[4] C. Eskilsson,[4] M.B. Kramer,[4,5] G. Papadakis,[6] and K. Nielsen[7]

1 National Renewable Energy Laboratory
2 Sandia National Laboratories
3 Basque Center for Applied Mathematics
4 Aalborg University
5 Floating Power Plant
6 National Technical University of Athens
7 Ramboll Group A/S

Suggested Citation
Tran, T.T., B.J. Meuris, C. Chartrand, J. Davidson, J. Andersen, C. Eskilsson, M.B. Kramer, G. Papadakis, and K. Nielsen. 2024. *High-Fidelity Numerical Wave Tank Verification & Validation Study: Wave Generation Through Paddle Motion: Preprint*. Golden, CO: National Renewable Energy Laboratory. NREL/CP-5700-90950. https://www.nrel.gov/docs/fy25osti/90950.pdf.

NREL is a national laboratory of the U.S. Department of Energy
Office of Energy Efficiency & Renewable Energy
Operated by the Alliance for Sustainable Energy, LLC

This report is available at no cost from the National Renewable Energy Laboratory (NREL) at www.nrel.gov/publications.

Contract No. DE-AC36-08GO28308

Conference Paper
NREL/CP-5700-90950
December 2024

National Renewable Energy Laboratory
15013 Denver West Parkway
Golden, CO 80401
303-275-3000 • www.nrel.gov

NOTICE

This work was authored in part by the National Renewable Energy Laboratory, operated by Alliance for Sustainable Energy, LLC, for the U.S. Department of Energy (DOE) under Contract No. DE-AC36-08GO28308. Funding provided by U.S. Department of Energy Office of Energy Efficiency and Renewable Energy Water Power Technologies Office. The views expressed herein do not necessarily represent the views of the DOE or the U.S. Government. The U.S. Government retains and the publisher, by accepting the article for publication, acknowledges that the U.S. Government retains a nonexclusive, paid-up, irrevocable, worldwide license to publish or reproduce the published form of this work, or allow others to do so, for U.S. Government purposes.

Cover Photos by Dennis Schroeder: (clockwise, left to right) NREL 51934, NREL 45897, NREL 42160, NREL 45891, NREL 48097, NREL 46526.

High-fidelity numerical wave tank verification & validation study: Wave generation through paddle motion

T. T. Tran
National Renewable Energy Laboratory, USA

B. J. Meuris & C. Chartrand
Sandia National Laboratories, USA

J. Davidson
Basque Center for Applied Mathematics, Spain

J. Andersen & C. Eskilsson
Aalborg University, Denmark

M. B. Kramer
Aalborg University, Denmark
Floating Power Plant, Denmark

G. Papadakis
National Technical University of Athens, Greece

K. Nielsen
Ramboll Group A/S, Denmark

ABSTRACT: This paper presents a numerical benchmark study of wave propagation due to a paddle motion using different high-fidelity numerical models, which are capable of replicating the nearly actual physical wave tank testing. A full time series of the measured wave generation paddle motion that was used to generate wave propagation in the physical wave tank will be utilized in each of the models contributed by the participants of International Energy Agency Ocean Energy Systems Task 10, which includes both computational fluid dynamics and smoothed particle hydrodynamics models. The high-fidelity simulations of the physical wave testcase will allow for the evaluation of the initial transient effects from wave ramp-up and its evolution in the wave tank over time for two representative regular waves with varying levels of nonlinearity. Metrics like the predicted wave surface elevation at select wave probes, wave period, and phase-shift in time will be assessed to evaluate the relative accuracy of numerical models versus experimental data within specified time intervals. These models will serve as a guide for modelers in the wave energy community and provide a base case to allow further and more detailed numerical modeling of the fixed Kramer Sphere Cases under wave excitation force wave tank testing.

1 INTRODUCTION

The International Energy Agency Technology Collaboration Programme for Ocean Energy Systems (OES) (IEA, 2022) has been working since 2001 to promote guidelines for the commercialization of wave energy converters (WECs). The initiative currently includes 25 member countries from around the world. In 2016, the OES Task 10 on numerical modeling and verification of WEC systems was approved to assess the accuracy and reliability of numerical models for all aspects of WEC development. Initial results and conclusions were reported in Wendt et al. (2019) for two single-degree-of-freedom point absorbers. This was followed by a study of a breakwater-mounted oscillating water column (OWC) device tested at large

scale (1:4) and reported in Bingham et al. (2021). In parallel, a set of highly accurate decay test experiments on a floating sphere were presented by Kramer et al. (2021) and Andersen (2023), providing benchmark results with small enough uncertainties to definitively quantify the accuracy of different numerical models.

This work is a continuous effort of numerical model validation for the sphere model using experimental wave tank studies at Aalborg University in Denmark in an effort to compile a rigorous and detailed set of benchmark cases called the *Kramer Sphere Cases*. As an extension of the decay testcase presented by Kramer et al. (2021), two new testcases for excitation forces on a fixed sphere exposed to regular waves were formulated. The first testcase, called the *Idealized Testcase*, considers a time period after the waves have been ramped up and are fully developed, and the inputs to the numerical simulations merely consist of the wave height and period for a set of regular waves (Kramer et al., 2023). A second testcase, called the *Physical Testcase*, provides the measured wave generator paddle motion as inputs to the simulations, leaving the wave evolution and propagation in the basin to be modeled by the numerical models (Kramer & Andersen, 2024). Computational fluid dynamics (CFD) simulations on the physical testcase will include initial transient effects from the wave ramp-up and the evolution of the wave in the basin over time. In contrast, CFD simulations on the idealized testcase will not include these effects. The physical testcase is divided into two studies:

- Comparison of waves in the basin without the model in place. Input is the paddle motion signal, and outputs are the waves at the wave gauge positions.

- Comparison of wave forces on the sphere. Input is the paddle motion signal, and output is the wave forces on the sphere.

The present work provides the results of initial efforts for the first study to model the waves in the basin using various high-fidelity models and a linear potential-based model.

2 SOLUTION VERIFICATION

Comparing the numerical results against experimental data is always recommended, but often no data are available to compare against. Solution verification is then the part of the verification and validation (V&V) procedure aiming to estimate the accuracy of a numerical solution when there is no exact solution to compare against. With regard to the wave energy sector, there are only a few works focusing on solution verification (Eskilsson et al., 2017; Brown et al., 2020; Amaral et al., 2022). Additionally, a number of studies have employed solution verification approaches to prove that the solutions presented are converged, e.g., Windt et al. (2020) and Katsidoniotaki & Göteman (2022). Recently, a comparison of four different solution verification methods was presented for the Kramer decay test (Eskilsson et al., 2023), and the method of Eça & Hoekstra (2014) was found to be the most versatile. The study also looked into different parameters to use in the assessment of uncertainty.

There are several approaches to V&V for CFD (Eça & Hoekstra, 2014; Roache, 1997; Stern et al., 2001; Oberkampf & Trucano, 2008), and there are also standards and recommendations (AIAA, 1998; ASME, 2009; ITTC, 2017). Using a sequence of refined meshes, the methods estimate the numerical convergence rate p and typically employ Richardson extrapolation to obtain an estimate of the value at zero grid spacing ϕ_0. Finally, the estimated numerical errors are converted into numerical uncertainty using safety factors.

The present study will use the least-square grid convergence index (GCI) method of Eça & Hoekstra (2014) to assess the numerical discretization errors and uncertainties. The parameters of interest include free surface wave elevation, wave period, and wave phase via time-shift at different measured wave gauges distributed along the wave tank. A complete solution verification also considers errors and uncertainties arising from iteration errors (e.g., outer iterations in a Semi-Implicit Method for Pressure Linked Equations (SIMPLE) scheme and convergence tolerances in the linear system solvers), modeling errors (e.g., turbulence), and geometric errors (e.g., simplified geometries and truncated numerical wave tank). However, in this study, the focus is on spatial and temporal errors, which usually are the dominating terms.

3 WAVE TANK MEASUREMENTS

The Ocean Energy Systems Technology Collaboration Programme has been performing experimental wave tank studies (shown in Figure 1) at Aalborg University in Denmark in an effort to compile a rigorous and detailed set of benchmark cases for numerical model validation. The test article consists of a rigid sphere, fixed in position, half submerged in water, and subjected to regular waves of three different levels of linearity (Andersen & Kramer, 2023).

The wave tank is $14.6 \times 19.3 \times 1.5$ m (internal length $\times$ width $\times$ wall height) with an active test area of 8.44×13.00 m (length $\times$ width). The basin is equipped with long-stroke segmented piston wavemakers for accurate short-crested (three-dimensional) random wave generation with active absorption. Only two-dimensional (2D) waves were generated in the present sphere tests, and active absorption was not included to have as good repeatability as possible. A

graphic of the wave tank dimensions and real wave basin is given in Figure 1.

As shown in the bottom graphics of Figure 1, nine wave gauges (WG) were placed in the tests that included the model: WG1–3 were placed along $y = 0$ at the wave generator side of the model with WG1 closest to the wave generator, WG4–6 were placed along $y = 0$ behind the model with WG6 closest to the beach, and WG7–9 were placed along $x = 0$ with WG7 closest to a sphere model (not shown in the graphic).

In tests where the waves were measured without the sphere model, three additional wave gauges, WG10–12, were included. WG11 was placed at the center of the sphere location, as shown in the sketch in the right part of Figure 1. The position of the wave gauges allows for studies such as the reflection characteristics.

4 NUMERICAL MODELS ADOPTED BY THE PARTICIPATING TEAMS

In this study, the results from seven high-fidelity CFD models solving the fully nonlinear and viscous unsteady Reynolds-averaged Navier-Stokes (URANS) equations are included. Smoothed particle hydrodynamics (SPH) models with two different boundary types—dynamic boundary dondition (DBC) and modified DBC (mDBC)—are also included. Additionally, one model based on the linear potential flow (LPF) theory is included to illustrate the capabilities of the standard linear theory. The paddle motion was modeled using the time history of the physical paddle position—sampled at 50 Hz—to specify the position of the moving paddle boundary. Linear interpolation was used to obtain the paddle position at the time steps specified by the numerical model, while mesh morphing is achieved by solving the Laplacian for the motion displacement within OpenFOAM-based solvers. Primary numerical settings of the different numerical models are described in Table 1.

4.1 *OpenFOAM-based Solvers*

The well-known open-source framework OpenFOAM is founded on the cell-centred finite volume method (FVM) (OpenCFD Ltd, 2024; Weller et al., 1998). OpenFOAM is shipped with a multitude of solvers, four of which are used in the present study.

4.1.1 *waveFoam Solver (SNL)*

WaveFoam solves the two-phase Navier-Stokes equations for incompressible, isothermal, and immiscible fluids with the free surface captured using the volume of fluid (VOF) method. WaveFoam uses an algebraic VOF and relies on the multidimensional universal limiter for explicit solution (MULES) and an interface compression scheme (Deshpande et al., 2012). A laminar simulation setup, which omits the use of a turbulence model, was specified. Implicit Euler was utilized for progressing the solution in time. Second-order, central differencing was used for the gradient operator while a corrected central difference scheme was used for the Laplacian operator. The divergence operators were specified as follows: vanLeer for $\nabla \cdot (\rho \boldsymbol{U}\boldsymbol{U})$; monotone upstream-centered schemes for conservation laws (MUSCL) for $\nabla \cdot (\boldsymbol{U}\alpha)$; interfaceCompression for $\nabla \cdot (\boldsymbol{U}_{rb}\alpha)$; central differencing for any terms not otherwise listed. Wave damping is achieved through the use of a relaxation zone, as outlined in Jacobsen et al. (2012).

4.1.2 *interFoam Solver (AAU)*

This solver is the same model as presented by SNL above, but with a couple of different settings in the numerical schemes. The main difference is that AAU uses second-order cell-limited central differencing as the gradient operator, i.e., the face values given by the gradient operator are bounded by the minimum and maximum of the neighboring cells. The limiter adds diffusion to advection and is thus not recommended for simulation of pure wave propagation. However, a limiter is often required to stabilize wave-body interaction problems. Thus, it is of interest to investigate the influence of the limiter. Additionally, the divergence operators are all of standard second-order vanLeer type. The paddle motion is simulated by reading in a table of the paddle position history to move the boundary accordingly, letting the mesh stretch under Laplacian smoothing. It should be noted that the mesh motion caused the second-order Crank-Nicholson time stepping scheme to become unstable, and implicit Euler had to be used.

4.1.3 *waveIsoFoam Solver (SNL)*

The main difference between the waveFoam and waveIsoFoam solvers are the use of algebraic versus geometric VOF. The waveIsoFoam model relies on the geometric VOF called isoAdvector as presented in Roenby et al. (2016). IsoAdvector reconstructs the interface inside the cells using an isosurface concept. Otherwise, the model uses the same settings as the SNL waveFoam setup, where applicable.

4.1.4 *potentialFreeSurfaceFoam Solver (BCAM)*

The potentialFreeSurfaceFoam solver is an adaptation of the pimpleFoam solver, which is commonly utilized for incompressible, single-phase, transient flow simulations. This adaptation incorporates a unique boundary condition known as waveSurfacePressure. This boundary condition calculates the change in surface elevation at each time step by using the volume flux for the cells at the top boundary. More information can be found in Schmitt et al. (2020).

(a)

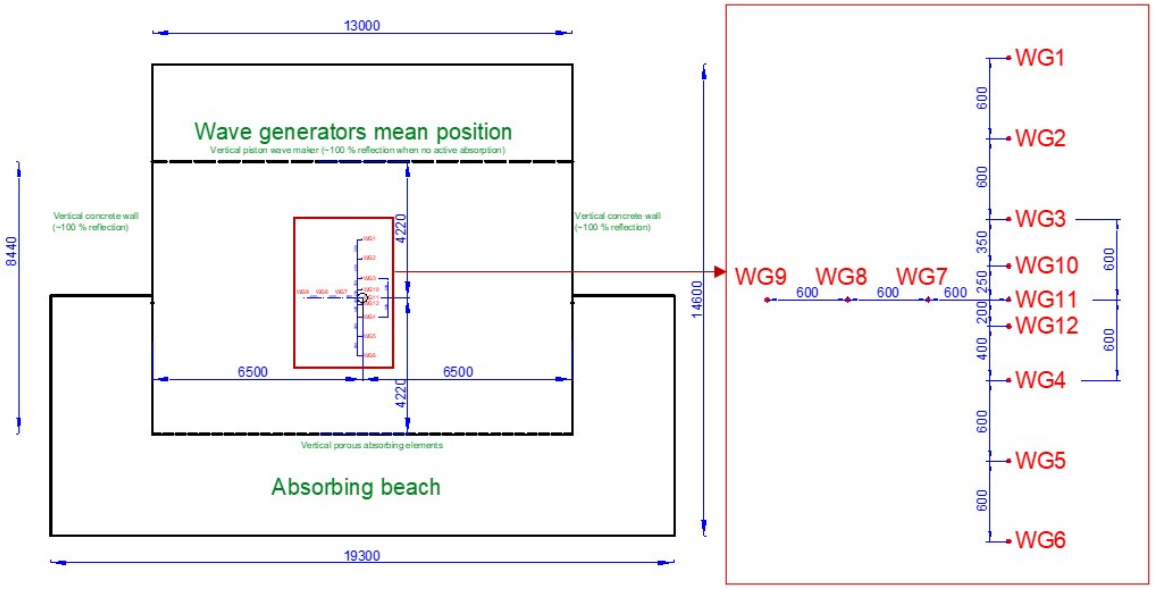

(b) (c)

Figure 1: Physical wave tank: (a) Real wave tank setup (b) Overall dimensions and its setup layout (unit in mm) (c) A detail of wave gauges's locations

4.2 *MaPFlow Solver (NTUA)*

MaPFlow is an URANS solver primarily developed at the NTUA. It is a cell centered CFD solver employing unstructured polyhedral grids. Incompressibility is treated using the artificial compressibility method (see Ntouras & Papadakis, 2020) while two-phase flows are modeled through VOF using the HRIC scheme. Regarding mesh deformation, MaPFlow utilizes a radial basis function approach (see Theodorakis et al., 2022).

4.3 *STAR-CCM+ Solver (NREL)*

Second-order schemes were chosen for both the spatial and temporal discretization. The SIMPLE approach was chosen to solve the pressure-velocity coupling with 20 iterations per time step. The under-relaxation factors for velocity and pressure are 0.9 and 0.4, respectively. A mesh morphing approach using the radial basis function technique was used to resolve the mesh deformation due to the time history input of paddle motion applied at the inlet boundary.

4.4 *DualSPhysics Solver (NREL)*

The DualSPHysics code (DualSPhysics, 2024) is an open-source Smoothed Particle Hydrodynamics (SPH) model which is a Lagrangian meshless method to discretize a continuum using a set of material points or particles. Specifically, the discretized Navier-Stokes equations are locally integrated at the location of each of the particles in the case of a fluid dynamic simulation. In this study, we applied both DBC and mDBC (DualSPhysics, 2024) for the numerical wave tank simulation. A variable time step and the second-order accurate Symplectic time integrator scheme were applied with a CFL-based value of 0.2. The Wendland model was selected for the smoothing kernel. An artificial viscosity of 0.01 was applied in this study. Four different mesh resolutions with the ratio of wave height and particle distances (H/D_p) of 7, 10, 15, and 20 were conducted for uncertainty quantification. The paddle motion in the physical tank testing was modeled by the piston motion via the experimental time history input.

4.5 *In-house Code using Linear Theory (AAU)*

The waves by the paddle use the analytical LPF solution for the piston-type wave maker *Biésel Transfer Function* presented by Biesel (1951). The interested reader can find a more recent description in English by Frigaard & Andersen (2010). Waves are propagated from the paddle to the actual position in the basin using linear wave theory by treating all the wave components as free waves. A script has been developed, which calculates the wave amplitude based on the simple analytical equation for the far field Biésel Transfer Function. The script is based on a frequency domain solution by making a fast Fourier transform of the measured paddle position, including the transfer functions on the individual components, and making an inverse fast Fourier transform to get the surface elevation at the specified points in the basin.

5 NUMERICAL TEST CASES

In the physical wave testing, various wave condition tests were conducted ranging from linear to highly nonlinear wave characteristics depending on wave steepness (Kramer et al., 2023; Kramer & Andersen, 2024). Although 12 wave cases were conducted, only two interesting wave conditions, R05 and R12, were selected in this study. The R05 wave case has an intermediate wave steepness, whereas the R12 wave case is the highest and steepest wave in the physical wave condition test set. Details of the selected wave conditions are given in Table 2.

In the low- and high-fidelity simulation models, these two wave conditions were simulated and compared with the physical wave tank results. The computational domain has the exact same length compared to the physical wave tank: 4.22 m and 7.37 m from WG11 (or the center of the sphere model) to the wave paddle and the end of tank, respectively. Without the sphere model in place, only one cell layer in the lateral direction was generated. The mesh resolution in the wave elevation regime was refined to capture wave propagation. For every wave case selected, five different spatial resolutions with the ratios of vertical cell size per wave height ($H/\Delta z$) by longitudinal cell size per wave length ($\lambda/\Delta x$) of 10×100, 15×100, 20×100, 20×150, and 20×200 were created and simulated with different temporal resolutions. That resulted in a mesh ratio between longitudinal and vertical cell size ($\Delta x/\Delta z$) that ranged from 1 to 4. An example of the mesh resolutions are graphically displayed in Figure 2. Three ratios of step size per wave period ($T/\Delta t$) of 500, 750, and 1000 were used in this study. A total of 15 simulations for each wave case were conducted. The selection of these time step sizes with respect to the mesh resolution at wave surface regime satisfies the Courant number less than 0.5. Overall, these spatial and temporal discretizations are well defined and are commonly used for numerical wave tank studies (Windt et al., 2018).

As the computational domain has only a single layer in the third direction (y-direction), the simulation is a 2D computational model. The inlet boundary was specified as a moving paddle with a prescribed time history motion extracted from the physical wave tank testing. The bottom surface was defined as a physical wall in the tank. During the simulation, a mesh morphing approach was applied to handle a grid deformation due to the moving inlet boundary. Wave elevation at different wave gauge locations (WG1,2,11) was simultaneously monitored and extracted. Subsequently, their time history data were sampled with the time interval of 0.01 s for data post-processing and analysis.

6 RESULTS AND DISCUSSION

This section presents a comparison of wave characteristics of the *Physical Testcases* between the physical and numerical wave tank testing. As mentioned, there are 15 simulations consisting of 5 different mesh resolutions and 3 different time step sizes for every wave case. It is noted that the results plotted and presented in this paper are of the finest spatial and temporal discretization.

The comparison of transient wave elevation between experimental data and numerical solutions at WG11 with respect to the wave cases R05 and R12 is graphically illustrated in Figure 3. The two top plots show the time history of wave elevation without a modified time shift. Overall, the results of most numerical models show good agreement with the physical wave tank result. As the wave case R05 has a shorter wave period, 0.88 s as shown in Table 2, it takes a longer time to reach expected wave elevation behavior at WG11.

The two bottom plots in Figure 3 present the comparison of wave elevation at interesting periods, which we selected to minimize the potential of wave reflection while achieving the expected stable wave elevation in the physical wave tank. These results were time-shifted, such that the data were adjusted to have the same wave elevation peak compared to the experimental data—10.9 s and 7.6 s for the wave case R05 and R12, respectively. The time domain data of this interesting regime were further processed and analyzed and are presented in this section. Specifically, two troughs, three crests, and their time locations extracted from the interesting data period were utilized for calculating averaged wave height, wave period, and time shift. These data comprising 15 simulations for every wave case are then used for uncertainty calculation and subsequently for V&V purposes. The least-square GCI method of Eça & Hoekstra (2014) to assess the numerical discretization errors and uncertainties was used in this study. Monotonic convergences were observed for all cases, as the maximum

Table 1: Primary numerical settings in different numerical models

Participant	Software	Domain Length		Pressure-Velocity Coupling					Boundary Conditions		Wave Forcing/Relaxation/Damping Zones		Turbulent Model	Volume Fraction Transport Scheme
					Stopping Criteria									
		Upstream Length	Downstream Length	Algorithm	No. of Pressure Correction	Residual Tolerance	Max. Interations/ nOuterCorrectors	nCorrectors	Upstream	Downstream	Upstream Type/Length	Downstream Type/Length		
NREL	STAR-CCM+ 15.06	Physical wave tank: 4.22m from wave paddle to interesting wave probe (WG#11)	Physical wave tank: 7.37m from interesting wave probe (WG#11) to the end tank	SIMPLE	N/A	None	20	N/A	Prescribed Paddle Motion	Const. Pressure	N/A	3.15 m - Wave damping	k-w SST	HRIC
NREL	DualSPHysics 5.2			SPH	N/A	N/A	N/A	N/A			N/A	3.15 m - Passive wave absorption	Artificial viscosity	Kernel function
SNL	waveFoam (v2106)			PIMPLE	1	None	1	3		p_rgh: zeroGradient U: uniform (0 0 0)	N/A	3.15 m - Wave relaxation zone	laminar	MULES
SNL	waveIsoFoam (v2106)			PIMPLE	1	None	1	3		p_rgh: zeroGradient U: uniform (0 0 0)	N/A	3.15 m - Wave relaxation zone	laminar	isoAdvector
BCAM	potentialFreeSurfaceFoam			PIMPLE	1	None	2	2		p_rgh: zeroGradient U: noSlip	N/A	3.15 m - None	laminar	N/A
AAU	InterFoam (v2212)			PIMPLE	1	N/A	3	1		zeroGradient	N/A	3.15 m -relaxation	laminar	vanLeer
AAU	In-house code (Linear Theory)			N/A	N/A	N/A	N/A	N/A		N/A	N/A	N/A	N/A	N/A
NTUA	In-house code(MaPFlow)			Artificial Compressibility	N/A	N/A	10					3.14m Wave damping	laminar	HRIC

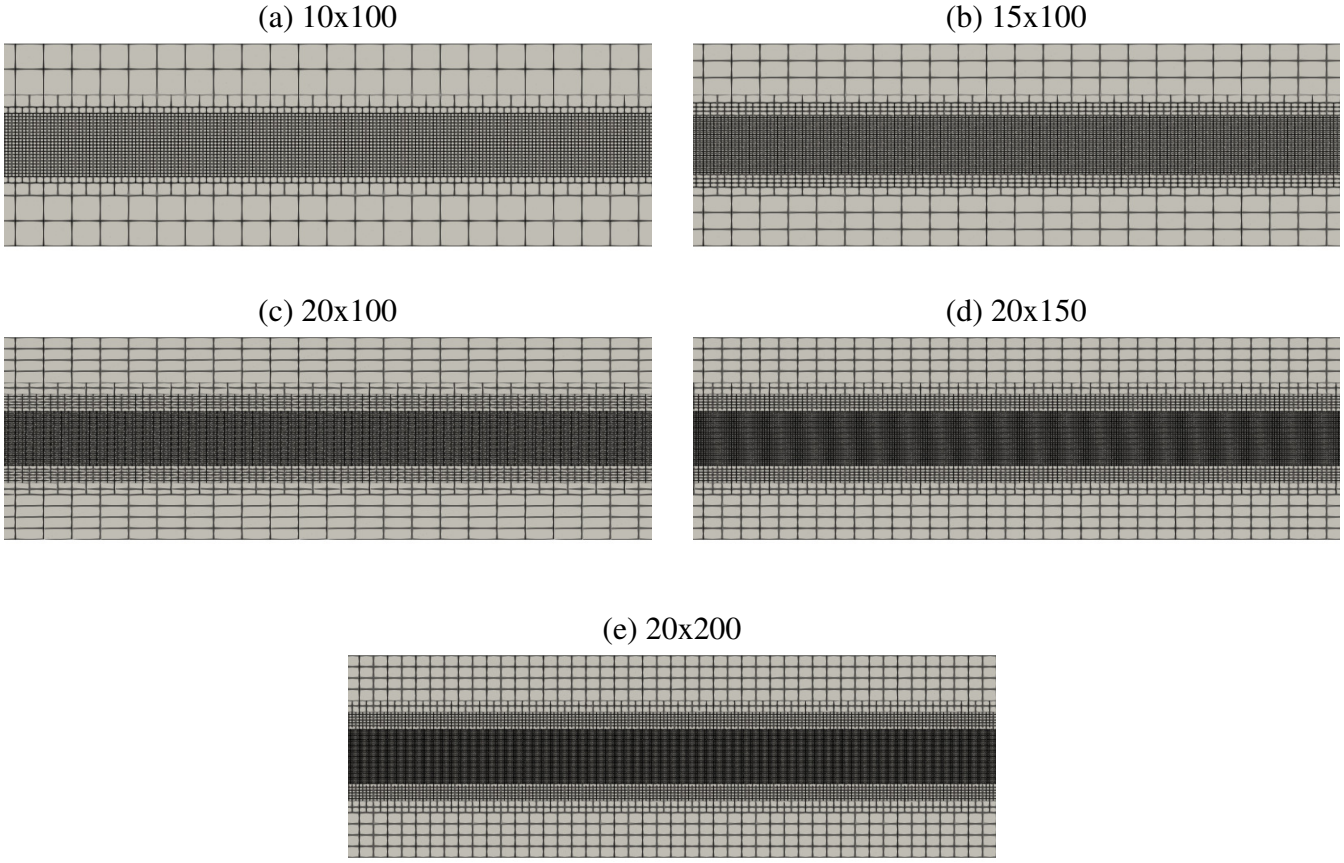

Figure 2: An example of mesh sequence of the wave case R12 used by the mesh-based URANS models.

Table 2: Selected wave condition

Case	Wave period T (s)	Wave height H (m)	Wave steepness H/λ (-)
R05	0.880	0.0561	0.0464
R12	1.420	0.2611	0.0829

order of accuracy for space (p) and time (q) of the fitting surface function is 2.

Figures 4 and 5 display the comparison of averaged wave height at different wave gauge locations (WG1-3,11) obtained by both physical and numerical wave tank testing. For the numerical wave tank testing, the bar plots represent the averaged wave height of the finest spatial and temporal resolution. The er-

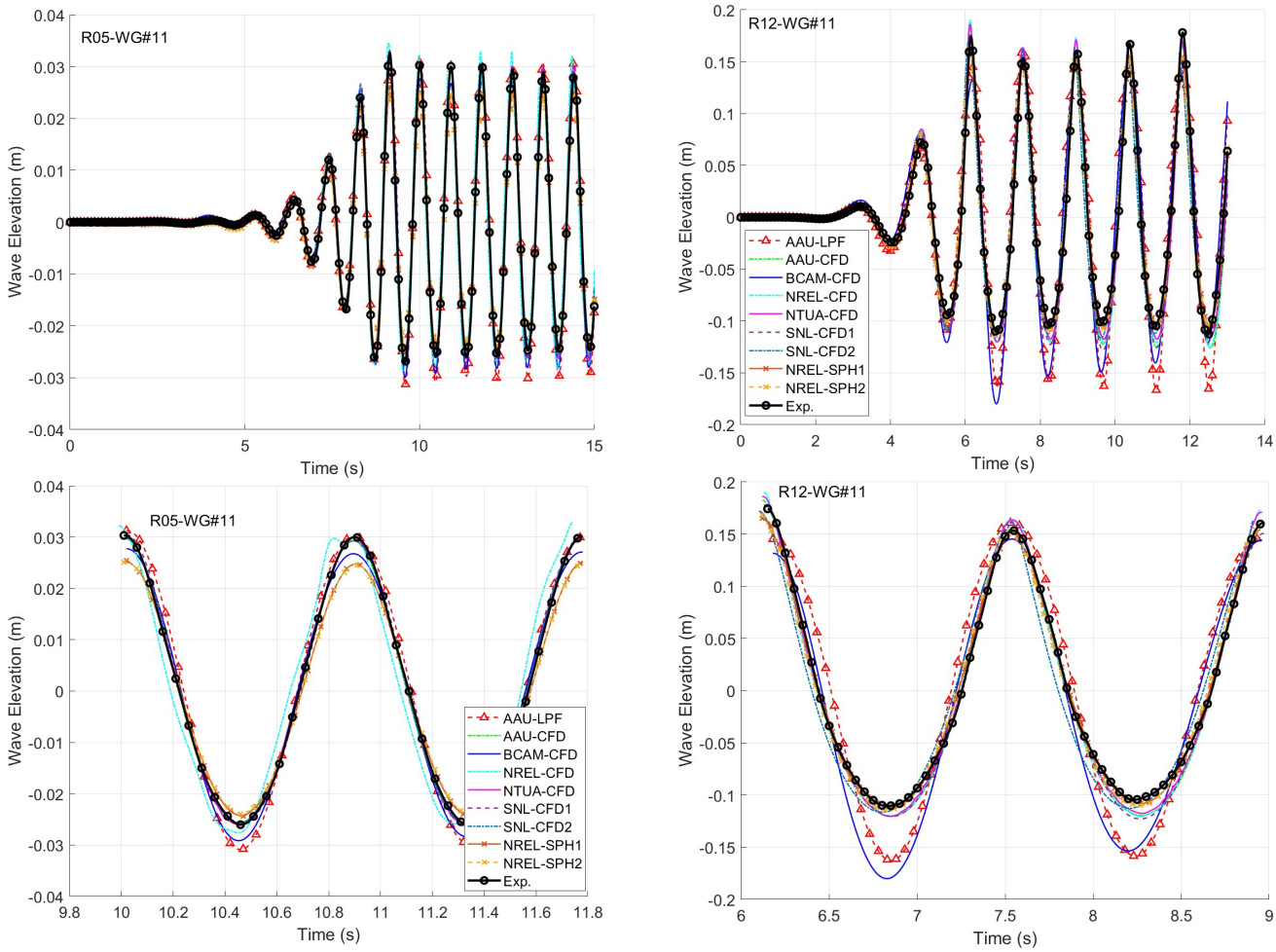

Figure 3: Comparison of the time history of wave elevation at WG11 with respect to two wave cases: full time history (top plots) and interested time period with matching peak location for data post-processing and analysis (bottom plots) (AAU-LPF: Linear potential flow; AAU-CFD: interFoam; BCAM-CFD: potentialFreeSurfaceFoam; NREL-CFD: STAR-CCM+; NTUA-CFD: MaPFlow; SNL-CFD1: waveFoam; SNL-CFD2: waveIsoFoam; NREL-SPH1: DBC; NREL-SPH2: mDBC).

ror bars represent uncertainty quantification, including both spatial and temporal metrics. For the experimental data, the error bar is calculated through 95% confidence interval. The uncertainty at WG11 is used for all other wave gauges plotted in this study.

Overall, the averaged wave heights predicted by the numerical wave tank models show good agreement compared to that of the physical wave tank. The wave height predicted by the linear potential-based theory including AAU-LPF and BCAM-CFD shows the largest discrepancy (R05: 8% and R12: 19%). However, numerical uncertainty of most high-fidelity models seems to be large, especially for the wave case R05 where the uncertainties varied from 32% (NREL-CFD) to 99% (NTUA-CFD). On the other hand, the experimental uncertainty is only 3.6%. Interestingly, the SPH models, especially the one with DBC boundary setting in this study has a small uncertainty with respect to the finest resolution. It is noted that the time step size in the SPH model is also changed with respect to the change of particle distance, as it is governed by the constant Courant–Friedrichs–Lewy (CFL) number of 0.2 in this study. It is also noted that all high-fidelity CFD solutions have the CFL number less 0.5 with the current spatial and temporal discretizations.

In the case of the highly nonlinear (highest and deepest steepness) wave case, R12, the agreement between physical and numerical wave tanks is better than that of the intermediate wave steepness case, R05. Uncertainties for this case varied from 4% (NTUA-CFD) to 47% (SNL-CFD2), whereas the uncertainty of the physical wave tank is 3%. Interestingly, NTUA-CFD's uncertainty result in the wave case R12 is lowest, whereas it is biggest in the wave case R05.

For the OpenFOAM-based solvers, there are slight differences, particularly for the *waveFoam* and *waveIsoFoam* solvers. Even for the similar *waveFoam* and *interFoam* solvers, a couple of different settings in the numerical schemes between AAU and SNL result in a slight difference in the uncertainty estimates. Between *waveFoam* and *waveIsoFoam* solvers, the discrepancy of uncertainty prediction is more deviated for the highly nonlinear wave case, R12.

As wave elevation is propagated from the inlet due to the paddle motion, the averaged wave period and its uncertainty calculated at different wave gauge locations behaves consistently among numerical models.

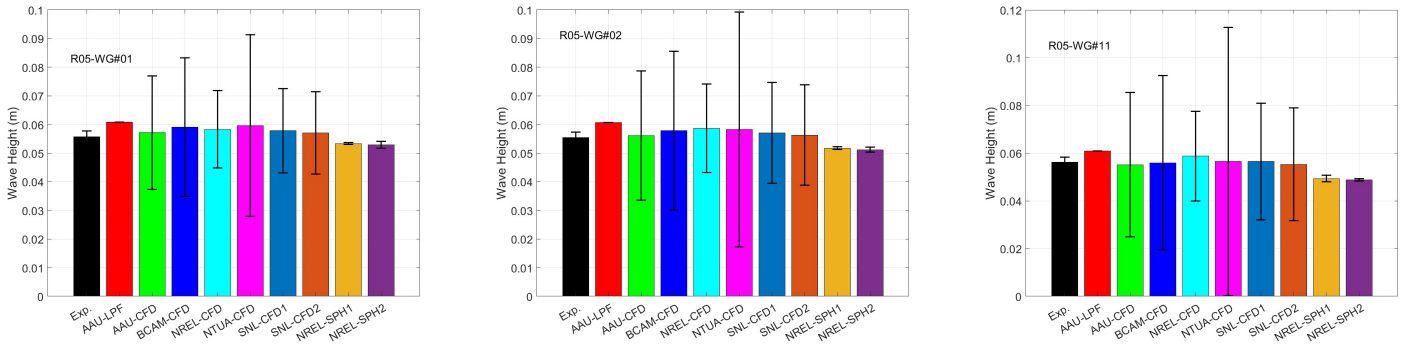

Figure 4: A comparison of averaged wave height between the physical and numerical wave tanks for the wave case R05.

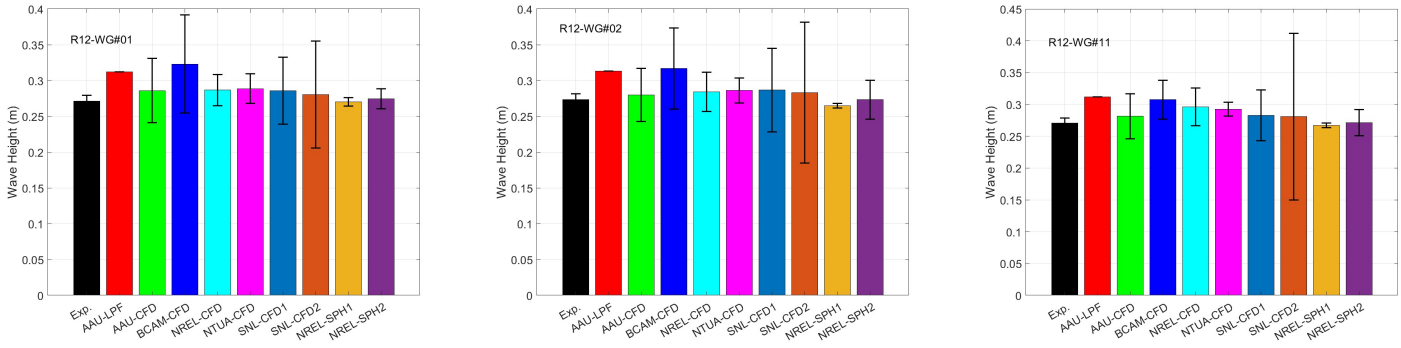

Figure 5: A comparison of averaged wave height between the physical and numerical wave tanks for the wave case R12.

Figures 6 and 7 display the comparison of averaged wave period predicted by different numerical models versus the physical wave tank. There is very good agreement between the physical and numerical wave tanks across the wave gauge locations with different wave cases. Most high-fidelity models also have small uncertainty estimates of wave period, except for the NREL-CFD model where the uncertainty is up to 14% for wave period estimates. Interestingly, both NREL-CFD (STAR-CCM+ solver) and SNL-CFD2 (waveIsoFoam) have quite similar uncertainty ranges across the wave gauge locations for the highly nonlinear wave case, R12.

7 CONCLUSIONS

This study presents an effort of V&V quantification of wave propagation considering the actual paddle motion in wave tank testing. This is a continuous effort of numerical model validation for the sphere model using experimental wave tank studies at Aalborg University in Denmark. Both low- and high-fidelity models, including different CFD models and SPH models, conducted and submitted by different participants are compared with the experimental data. The study applied the least-square GCI method of Eça & Hoekstra (2014) to assess the numerical discretization errors and uncertainties. Several metrics, including averaged wave height, averaged wave period, and time-shift (phase shift), extracted from an interesting data period across different wave gauge locations were assessed and evaluated for both intermediate and high wave steepness cases. Overall, we observed good agreement of wave elevation prediction between the physical and numerical wave tanks. Although the spatial and temporal discretizations in this study are appropriately defined in terms of the satisfaction of CFL number at the wave surface regime, numerical error and uncertainty of most high-fidelity CFD solvers are unexpectedly high. This results in the need for more investigations on V&V efforts using high-fidelity numerical wave tank studies for the wave propagation, considering the real paddle motion in the physical wave tank.

ACKNOWLEDGEMENT

Josh Davidson is funded by MCIN and by the European Union NextGenerationEU/PRTR-C17.I1, as well as by IKUR Strategy under the collaboration agreement between Ikerbasque and BCAM on behalf of the Department of Education of the Basque Government.

The Danish participants acknowledge the support given by the Danish Energy Technology Development and Demonstration Program (EUDP) under project number 134232-510153.

Sandia National Laboratories is a multi-mission laboratory managed and operated by National Technology & Engineering Solutions of Sandia, LLC (NTESS), a wholly owned subsidiary of Honeywell International Inc., for the U.S. Department of Energy's Na-

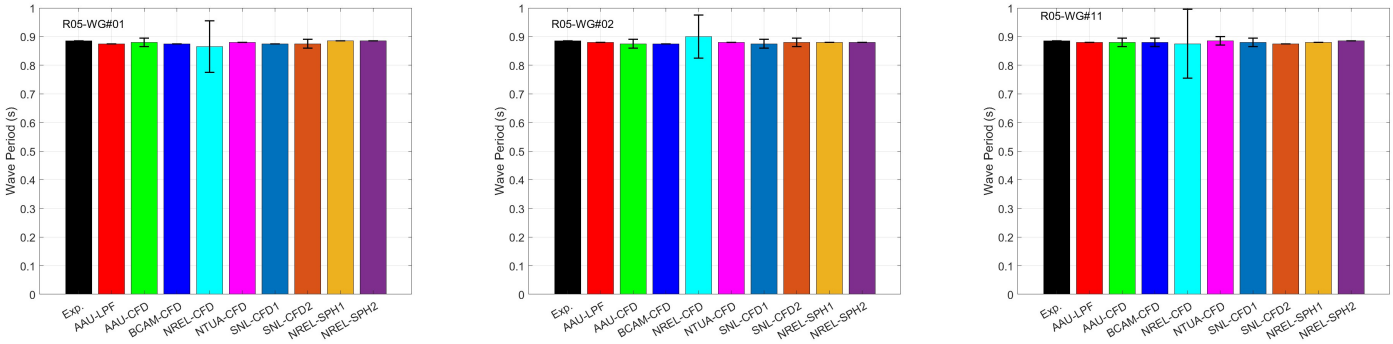

Figure 6: A comparison of averaged wave period between the physical and numerical wave tanks for the wave case R05.

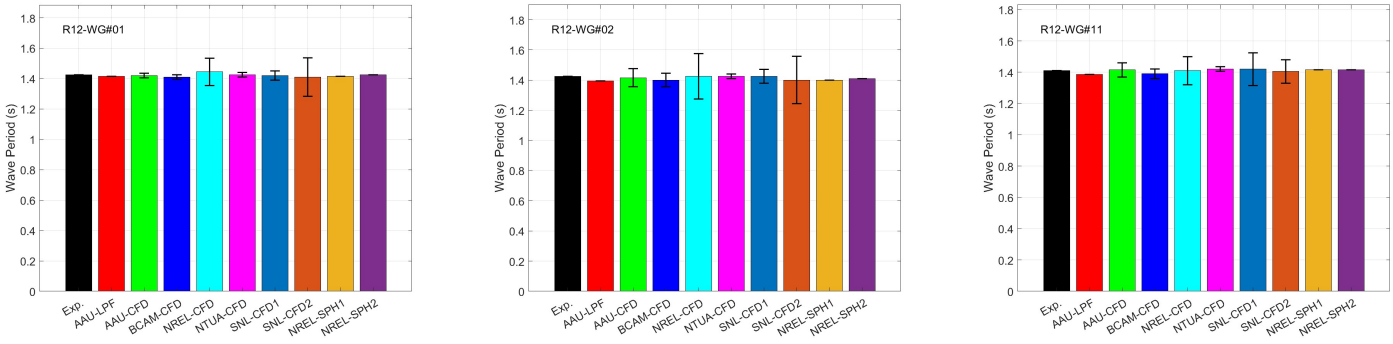

Figure 7: A comparison of averaged wave period between the physical and numerical wave tanks for the wave case R12.

tional Nuclear Security Administration (DOE/NNSA) under contract DE-NA0003525. This written work is authored by an employee of NTESS. The employee, not NTESS, owns the right, title and interest in and to the written work and is responsible for its contents.

This work was authored in part by the National Renewable Energy Laboratory, operated by Alliance for Sustainable Energy, LLC, for the U.S. Department of Energy (DOE) under Contract No. DE-AC36-08GO28308. Funding provided by U.S. Department of Energy Office of Energy Efficiency and Renewable Energy Water Power Technologies Office.

This effort is also supported by the U.S. Department of Energy's Water Power Technologies Office through the Testing Expertise and Access for Marine Energy Research (TEAMER) program.

This paper describes objective technical results and analysis. Any subjective views or opinions that might be expressed in the paper do not necessarily represent the views of the U.S. Department of Energy or the U.S. Government. The publisher acknowledges that the U.S. Government retains a non-exclusive, paid-up, irrevocable, world-wide license to publish or reproduce the published form of this written work or allow others to do so, for U.S. Government purposes. The DOE will provide public access to results of federally sponsored research in accordance with the DOE Public Access Plan.

REFERENCES

AIAA (1998). "Guide for Verification and Validation of Computational Fluid Dynamics Simulations". In: *AIAA Standards* AIAA G-077-1998.

Amaral, T., M. Rentschler, G. Vaz & J. Baltazar (2022). "Comprehensive Verification and Validation of a CFD Analysis". In: vol. Volume 8: Ocean Renewable Energy. International Conference on Offshore Mechanics and Arctic Engineering. DOI: 10.1115/OMAE2022-80578.

Andersen, J. (2023). *Hydrodynamic Modelling of Offshore Renewables: Experimental Benchmark Datasets and Numerical Simulation*. DOI: 10.54337/aau620115007.

Andersen, J. & M. B. Kramer (2023). "Wave excitation tests on a fixed sphere: Comparison of physical wave basin setups". In: *Proceedings of the European Wave and Tidal Energy Conference*. Vol. 15.

ASME (2009). *Standard for Verification and Validation in Computational Fluid Dynamics and Heat Transfer*. Standard No. V V20. American Society of Mechanical Engineers.

Biesel, F. (1951). "Les apparails generateurs de houle en laboratoire". In: *La Houille Blanche* 6, p. 4.

Bingham, H. B. et al. (2021). "Ocean Energy Systems wave energy modelling task 10.4: Numerical modelling of a fixed oscillating water column". In: *Energies* 14 (6), p. 1718. DOI: 10.3390/en14061718.

Brown, S. A., E. J. Ransley, P.-H. Musiedlak & D. Greaves (2020). "Quantifying the Predictive Capability of OpenFOAM 5.0: Focused Wave Impacts with Floating Bodies". In: *International Journal of Offshore and Polar Engineering* 30.01, pp. 20–27. DOI: 10.17736/ijope.2020.jc779.

Deshpande, S. S., L. Anumolu & M. F. Trujillo (2012). "Evaluating the performance of the two-phase flow solver interFoam". In: *Computational science & discovery* 5.1, p. 014016.

DualSPhysics (2024). *https://github.com/DualSPHysics/DualSPHysics/wiki*.

Eça, L. & M. Hoekstra (2014). "A procedure for the estimation of the numerical uncertainty of CFD calculations based on grid refinement studies". In: *Journal of Computational Physics* 262, pp. 104–130.

Eskilsson, C., J. Palm & L. Bergdahl (2017). "On numerical uncertainty of VOF-RANS simulations of wave energy converters through V&V techniques". In: *Proceedings of the 12th European Wave and Tidal Energy Conference (EWTEC2017)*. Cork, Ireland.

Eskilsson, C., A. Shiri & E. Katsidoniotaki (2023). "Solution verification of WECs: comparison of methods to estimate numerical uncertainties in the OES wave energy modelling task". In: *Proceedings of the 15th European Wave and Tidal Energy Conference (EWTEC2023)*. Bilbao, Spain.

Frigaard, P. & T. Andersen (2010). *Technical Background Material for the Wave Generation Software AwaSys 5*. DCE Technical reports 64. Denmark: Department of Civil Engineering, Aalborg University.

IEA (2022). *OES - Ocean Energy Systems, an International Energy Agency Technology Initiative*.

ITTC (2017). *ITTC Quality Manual, Uncertainty Analysis in CFD*. Recommended Procedures and Guidelines. International Towing Tank Conference.

Jacobsen, N. G., D. R. Fuhrman & J. Fredsøe (2012). "A wave generation toolbox for the open-source CFD library: OpenFoam®". In: *International Journal for numerical methods in fluids* 70.9, pp. 1073–1088.

Katsidoniotaki, E. & M. Göteman (2022). "Numerical modeling of extreme wave interaction with point-absorber using OpenFOAM". In: *Ocean Engineering* 245, p. 110268. DOI: https://doi.org/10.1016/j.oceaneng.2021.110268.

Kramer, M. et al. (2021). "Highly accurate experimental heave decay tests with a floating sphere: A publich benchmark dataset for model validation of fluid-structure interaction". In: *Energies* 14, p. 269. DOI: https://doi.org/10.3390/en14020269.

Kramer, M. & J. Andersen (2024). *Wave Excitation Forces on a Sphere: Description of a Physical Testcase*. 3rd ed. DCE Technical Reports 308. Department of the Built Environment, Aalborg University.

Kramer, M., J. Andersen & K. Nielsen (2023). *Wave Excitation Forces on a Sphere: Description of an Idealized Testcase*. 2nd ed. DCE Technical Reports 307. Department of the Built Environment, Aalborg University.

Ntouras, D. & G. Papadakis (2020). "A coupled artificial compressibility method for free surface flows". In: *Journal of Marine Science and Engineering* 8.8, p. 590.

Oberkampf, W. L. & T. G. Trucano (2008). "Verification and validation benchmarks". In: *Nuclear Engineering and Design* 238.3, pp. 716–743.

OpenCFD Ltd (2024). *www.openfoam.com*.

Roache, P. J. (1997). "Quantification of Uncertainty in computational fluid dynamics". In: *Annual Review of Fluid Mechanics* 29, pp. 123–160.

Roenby, J., H. Bredmose & H. Jasak (2016). "A computational method for sharp interface advection". In: *R. Soc. open sci.* 3, pp. 160405–160405. DOI: http://doi.org/10.1098/rsos.160405.

Schmitt, P., C. Windt, J. Davidson, J. V. Ringwood & T. Whittaker (2020). "Beyond VoF: alternative OpenFOAM solvers for numerical wave tanks". In: *Journal of ocean engineering and marine energy* 6, pp. 277–292.

Stern, F., R. V. Wilson, H. W. Coleman & E. G. Paterson (2001). "Comprehensive Approach to Verification and Validation of CFD Simulations – Part 1: Methodology and Procedures". In: *Journal of Fluids Engineering* 123, pp. 793–802.

Theodorakis, K., D. Ntouras & G. Papadakis (2022). "Investigation of a submerged fully passive energy-extracting flapping foil operating in sheared inflow". In: *Journal of Fluids and Structures* 113, p. 103674.

Weller, H., G. Tabor, H. Jasak & C. Fureby (1998). "A tensorial approach to computational continuum mechanics using object-oriented techniques". In: *Computers in Physics* 12.6, pp. 620–631.

Wendt, F. et al. (2019). "Ocean energy systems wave energy modelling task: modelling, verification and validation of wave energy converters". In: *J. Marine Science and Eng.* 7 (11), p. 22.

Windt, C., J. Davidson & J. V. Ringwood (2018). "High-fidelity numerical modelling of ocean wave energy systems: A review of computational fluid dynamics-based numerical wave tanks". In: *Renewable and Sustainable Energy Reviews* 93, pp. 610–630.

Windt, C., J. Davidson, P. Schmitt & J. V. Ringwood (2020). "Wave–structure interaction of wave energy converters: a sensitivity analysis". In: *Proceedings of the Institution of Civil Engineers - Engineering and Computational Mechanics* 173.3, pp. 144–158. DOI: 10.1680/jencm.19.00033.